$\sigma-\pi^*$ Electronic Transition of the Di- and Trinuclear Complexes Ru(E)(E′)$(CO)_2$(iPr-DAB): Resonance Raman, Electronic Absorption, Emission, and Density Functional Study (E = Me, $SnPh_3$, $M(CO)_5$; E′ = $M(CO)_5$; M = Mn, Re; iPr-DAB = *N*,*N*′-Diisopropyl-1,4-diaza-1,3-butadiene)

Maxim P. Aarnts, Maikel P. Wilms, and Derk J. Stufkens*,†

Anorganisch Chemisch Laboratorium, J. H. van't Hoff Research Institute, Universiteit van Amsterdam, Nieuwe Achtergracht 166, 1018 WV Amsterdam, The Netherlands

Evert Jan Baerends

Afdeling Theoretische Chemie, Vrije Universiteit, De Boelelaan 1083, 1081 HV Amsterdam, The Netherlands

Antonín Vlček, Jr.*,‡

J. Heyrovský Institute of Physical Chemistry, Academy of Sciences of the Czech Republic, Dolejškova 3, 182 23 Prague, Czech Republic, and Department of Chemistry, Queen Mary and Westfield College, University of London, London E1 4NS, U.K.

Received October 11, 1996⊗

Di- and trinuclear complexes Ru(E)(E′)$(CO)_2$(iPr-DAB) (E = Me, $SnPh_3$, $Mn(CO)_5$, E′ = $Mn(CO)_5$; E = Me, $SnPh_3$, $Re(CO)_5$, E′ = $Re(CO)_5$; iPr-DAB = *N*,*N*′-diisopropyl-1,4-diazabutadiene), which contain Ru−Mn or Ru−Re σ bonds, absorb strongly in the visible spectral region. A combined spectroscopic (absorption and resonance Raman) and theoretical (DFT-MO) study shows that the lowest allowed electronic transition has a $\sigma_{(Ru-E)} \rightarrow \pi^*_{(DAB)}$ or $\sigma_{n(E-Ru-E')} \rightarrow \pi^*_{(DAB)}$ character. The latter transition originates in a σ orbital, which is only weakly bonding or even nonbonding (σ_n) with respect to the axial E−Ru−E′ bonds. The second visible absorption band that occurs at higher energies for $Ru(M(CO)_5)_2(CO)_2$-(iPr-DAB) (M = Mn, Re) is attributed to a $\sigma_b \rightarrow \pi^*$ transition, the electron being excited from a strongly E−Ru−E′ σ-bonding orbital. Both $\sigma \rightarrow \pi^*$ transitions of the trinuclear complexes have surprisingly high oscillator strengths (0.1−0.2). An emission study of Ru-(E)(E′)$(CO)_2$(iPr-DAB) shows that their lowest excited state has a $^3\sigma\pi^*$ character. The emission is rather long lived (4−100 μs at 80 K, depending on the complex composition) because of slow nonradiative decay to the ground state.

1. Introduction

The photochemical and photophysical behavior of the complexes *trans*,*cis*-Ru(E)(E′)$(CO)_2$(iPr-DAB) (E = Me, E′ = Otf, Cl, Br, I, $Mn(CO)_5$; E = Et, iPr, E′ = I (see Figure 1)) was recently shown to depend strongly on the properties of the ligands E and E′ and their particular combination.[1] Thus, complexes containing an ethyl or methyl ligand in combination with a halide have a lowest Ru → diimine (MLCT) or halide → diimine (XLCT) excited state which is hardly reactive.[2] On the other hand, complexes containing an I/iPr or Me/Mn-$(CO)_5$ combination of the axial ligands E,E′ react photochemically by a homolytic splitting of the Ru−iPr or Ru−$Mn(CO)_5$ bond, respectively, just as the related compounds Re(E)$(CO)_3$(α-diimine) (E = ethyl, $Mn(CO)_5$, etc.).[3,4]

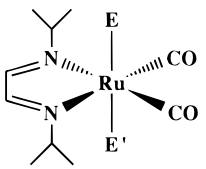

Figure 1. Schematic structure of Ru(E)(E′)$(CO)_2$(iPr-DAB).

This photochemical M−E bond homolysis does not occur from a $^3\sigma\sigma^*$ excited state, like in $Re_2(CO)_{10}$ or Mn_2-$(CO)_{10}$,[5] but from a reactive $^3\sigma\pi^*$ excited state, in which an electron is excited from the σ(M−E) bonding orbital to the lowest π^* orbital of the diimine ligand.[6] In the former case of the $\sigma\sigma^*$ reactivity, the M−M bond splitting in $Mn_2(CO)_{10}$ and $Re_2(CO)_{10}$ is completed on a subpicosecond time scale,[7] whereas the reaction observed for the α-diimine-substituted complexes often

* To whom correspondence should be addressed.
† E-mail: stufkens@anorg.chem.uva.nl.
‡ E-mail: vlcek@jh-inst.cas.cz or a.vlcek@qmw.ac.uk. Address correspondence to the University of London.
⊗ Abstract published in *Advance ACS Abstracts,* April 1, 1997.
(1) Nieuwenhuis, H. A.; Stufkens, D. J.; Vlček, A., Jr. *Inorg. Chem.* **1995**, *34*, 3879.
(2) Nieuwenhuis, H. A.; Stufkens, D. J.; McNicholl, R.; Al-Obaidi, A. H.; Coates, C. G.; Bell, S. E. J.; McGarvey, J. J.; Westwell, J.; George, M. W.; Turner, J. J. *J. Am. Chem. Soc.* **1995**, *117*, 5579.
(3) Rossenaar, B. D.; Kleverlaan, C. J.; van de Ven, M. C. E.; Stufkens, D. J.; Oskam, A.; Goubitz, K.; Fraanje, J. *J. Organomet. Chem.* **1995**, *493*, 153.
(4) Rossenaar, B. D.; George, M. W.; Johnson, F. P. A.; Stufkens, D. J.; Turner, J. J.; Vlček, A., Jr. *J. Am. Chem. Soc.* **1995**, *117*, 11582.
(5) Meyer, T. J.; Caspar, J. V. *Chem. Rev.* **1985**, *85*, 187.
(6) Rossenaar, B. D.; Lindsay, E.; Stufkens, D. J.; Vlček, A., Jr. *Inorg. Chim. Acta.* **1996**, *250*, 5.

S0276-7333(96)00866-7 CCC: $14.00

takes place from an excited state which is long lived (nanosecond or even microsecond) in apolar solvents.[8,9] Evidence for the presence of a lowest $^3\sigma\pi^*$ excited state is mainly obtained from its emission, which usually occurs with a small apparent Stokes shift and a relatively long lifetime, as well as from its characteristic transient absorption in the UV−vis and IR regions. It now becomes more and more apparent that the presence of a $^3\sigma\pi^*$ excited state is a common feature for complexes containing both a ligand covalently bound by a high-lying σ orbital and an electron-accepting ligand, like α-diimine. Hence, detailed knowledge of the nature and dynamics of $\sigma\pi^*$ states and of the mechanism of their population is of great importance. As for the latter aspect, it is still not quite clear whether the $\sigma\pi^*$ state is optically accessible or if it may only be populated via the primarily excited MLCT state(s). The former mechanism was suggested, *e.g.*, for $Zn(R)_2$(α-diimine) (R = alkyl)[10] and $Pt(Me)_4$(α-diimine)[11,12] complexes, whereas the latter, indirect population, was proposed for Re(E)-$(CO)_3$(iPr-DAB) (E = alkyl, $Mn(CO)_5$, $Re(CO)_5$, $SnPh_3$)[3,4,8] and Ru(Me)$(Mn(CO)_5)(CO)_2$(iPr-DAB).[9,13]

Quite remarkable results were obtained recently for the inorganometallic di- and trinuclear complexes Ru-(E)(E′)$(CO)_2$(iPr-DAB) (E = $SnPh_3$, E′ = Me, $SnPh_3$, $SnMe_3$, $GePh_3$; E = $PbPh_3$, E′ = Me, $PbPh_3$, $PbMe_3$, $GePh_3$).[14,15] In these complexes, the ligands E and E′ are in axial positions and σ-bonded to Ru. The lowest electronic transition appeared to be strongly allowed and to have $\sigma_{(E-Ru-E')} \rightarrow \pi^*_{(DAB)}$ character. This conclusion was derived from spectroscopic data and from the results of density functional (DFT) molecular orbital calculations. Photophysical studies on these complexes showed that the lowest $^3\sigma\pi^*$ state is a bound state whose lifetime is strongly influenced by E and E′. An exceptionally long lifetime of 264 μs was found for the $^3\sigma_{(Sn-Ru-Sn)}\pi^*$ state of the symmetrically substituted complex $Ru(SnPh_3)_2(CO)_2$(iPr-DAB) in a glass at 80 K.[15] For comparison, this lifetime is nearly a factor of 1000 longer than that of the ^{3}MLCT state of the closely related complex Ru(Cl)(Me)$(CO)_2$(iPr-DAB), which has about the same energy.[1]

Apparently, these novel complexes are really good emitters and may be good candidates for the development of a new class of luminophores or photosensitizers. To find out if this behavior is a general property of complexes of the type Ru(E)(E′)$(CO)_2$(α-diimine) (E = E′), we have extended our investigations to similar systems in which E and/or E′ represent a $Mn(CO)_5$ or $Re(CO)_5$ group. The σ orbitals of these $M(CO)_5$ groups are higher in energy than those of $SnPh_3$ and related group 14 ligands, suggesting a prominent role of the $\sigma\pi^*$ states in the photophysics and photochemistry of their Ru(E)(E′)$(CO)_2$(iPr-DAB) complexes. In this article, we present the UV−vis absorption, resonance Raman, and emission spectra of the complexes Ru(E)(E′)$(CO)_2$(iPr-DAB) (E = Me, $SnPh_3$, $M(CO)_5$; E′ = $M(CO)_5$; M = Mn, Re). Interpretation of the experimental results is aided by a DFT study of the molecular orbitals and electronic transitions of two model complexes, *viz.*, Ru(Me)(Mn-$(CO)_5)(CO)_2$(H-DAB) and Ru$(Mn(CO)_5)_2(CO)_2$(H-DAB). This DFT method was used since it is very fast compared to *ab initio* calculations and has been shown to provide accurate geometries and dissociation and excitation energies for transition metal complexes.[14−21]

2. Experimental Section

2.1. Materials and Preparations. THF (p.a.), 2-MeTHF (p.a.), and hexane (p.a) were obtained from Acros Chimica and were freshly distilled from sodium wire and handled under a N_2 atmosphere. Synthesis and characterization (^{1}H NMR, ^{13}C NMR, IR, UV−vis, and mass spectroscopy) of the complexes studied have been described elsewhere.[22]

2.2. Spectroscopic Measurements. Electronic absorption spectra were recorded on a Varian Cary 4E spectrophotometer. IR spectra were obtained on a Bio-Rad FTS-A60 FTIR spectrometer equipped with a liquid nitrogen-cooled MCT detector. Resonance Raman spectra of the samples, prepared as KNO_3 pellets, were measured on a Dilor XY spectrometer with a multichannel diode array detection system. A Spectra Physics 2016 Ar^+ laser was used as excitation source. To avoid photodecomposition during the Raman measurement, the pellet was kept spinning, and the exciting laser beam was directed on it through a rotating prism. The Raman spectra were corrected for the emission of the complexes and recalibrated for the excitation wavelength-dependent diode array shift using Grams software.[23] Emission and excitation spectra were measured using a Spex Fluorolog II emission spectrometer with a RCA-C31034 GaAs photomultiplier. The samples used for emission spectroscopy were dissolved in freshly distilled 2-MeTHF, freeze−pump−thaw degassed, and sealed off under vacuum in a cylindrical cuvette ($\phi \approx 1$ cm). The concentration was chosen such that the maximum absorbance in the spectral region investigated did not exceed 0.2. Low-temperature UV−vis and IR measurements were carried out in an Oxford Instruments DN 1704/54 liquid nitrogen cryostat, equipped with a NaCl, CaF_2, or quartz window.

2.3. Time-Resolved Spectroscopy. The detailed experimental setup for the time-resolved emission measurements has been described elsewhere.[24] Low-temperature measurements (77 K) in 2-MeTHF glasses were performed in an Oxford Instruments DN 1704/54 liquid nitrogen cryostat.

(7) Kim, S. K.; Pedersen, S.; Zewail, A. H. *Chem. Phys. Lett.* **1995**, *233*, 500.
(8) Rossenaar, B. D.; Kleverlaan, C. J.; van de Ven, M. C. E.; Stufkens, D. J.; Vlček, A., Jr. *Chem.-Eur. J.* **1996**, *2*, 228.
(9) Nieuwenhuis, H. A.; van Loon, A.; Moraal, M. A.; Stufkens, D. J.; Oskam, A.; Goubitz, K. *J. Organomet. Chem.* **1995**, *492*, 165.
(10) Kaupp, M.; Stoll, H.; Preuss, H.; Kaim, W.; Stahl, T.; van Koten, G.; Wissing, E.; Smeets, W. J. J.; Spek, A. L. *J. Am. Chem. Soc.* **1991**, *113*, 5606.
(11) Hasenzahl, S.; Hausen, H.; Kaim, W. *Chem.-Eur. J.* **1995**, *1*, 95.
(12) Hux, J. E.; Puddenphatt, R. J. *J. Organomet. Chem.* **1992**, *437*, 251.
(13) Nieuwenhuis, H. A.; van Loon, A.; Moraal, M. A.; Stufkens, D. J.; Oskam, A.; Goubitz, K. *Inorg. Chim. Acta* **1995**, *232*, 19.
(14) Aarnts, M. P.; Hartl, F.; Peelen, K.; Stufkens, D. J.; Fraanje, J.; Goubitz, K.; Wilms, M.; Baerends, E. J.; Vlček, A., Jr. *Inorg. Chem.* **1996**, *35*, 5468.
(15) Aarnts, M. P.; Wilms, M.; Stufkens, D. J.; Baerends, E. J.; Clark, I.; George, M. W.; Turner, J. J.; Vlček, A., Jr. *Chem.-Eur. J.* **1996**, *2*, 1556.
(16) Ziegler, T.; Rauk, A.; Baerends, E. J. *Theor. Chim. Acta* **1977**, *43*, 261.
(17) Ziegler, T.; Tschinke, V.; Versluis, L.; Baerends, E. J.; Revenek, W. *Polyhedron* **1988**, *7*, 1625.
(18) Rosa, A.; Ricciardi, G.; Baerends, E. J.; Stufkens, D. J. *Inorg. Chem.* **1995**, *34*, 3425.
(19) Rosa, A.; Ricciardi, G.; Baerends, E. J.; Stufkens, D. J. *J. Phys. Chem.* **1996**, *100*, 15340.
(20) Rosa, A.; Ricciardi, G.; Baerends, E. J.; Stufkens, D. J. *Inorg. Chem.* **1996**, *35*, 2886.
(21) Wilms, M. P.; Baerends, E. J.; Rosa, A.; Stufkens, D. J. *Inorg. Chem.* In press.
(22) Aarnts, M. P.; Stufkens, D. J.; Oskam, A.; Fraanje, J.; Goubitz, K.; Veldman, N.; Spek, A. L. *J. Organomet. Chem.*, in press.
(23) *Grams/386 implemented in WIN-IR software*; Galactic Industries Corp., Salem, NH, and Digilab Division, Bio-Rad Laboratories, Hercules, CA, 1991−1993.
(24) Rossenaar, B. D.; Stufkens, D. J.; Vlček, A., Jr. *Inorg. Chem.* **1996**, *35*, 2902.

Emission lifetimes (τ) were determined from the spectra measured at 20 progressive delay times (t) by fitting the decay of the emission intensity (I) at, at least, 10 different emission wavelengths to first-order kinetics ($I_t = I_0 \exp(-t/\tau)$). Emission quantum yields (Φ_{em}) were measured using solutions with an absorbance <0.2 at 460 nm relative to a standard solution of $Re(Cl)(CO)_3(bpy)$.[25] The necessary corrections were applied.[26,27] All calculations on the spectra (determination of τ, Φ_{em}, etc.) were performed with Grams software.[23]

2.4. Computational Details. All calculations were performed using the Amsterdam Density Functional program package ADF.[28,29] The computational scheme is characterized by the use of a density fitting procedure to obtain accurate Coulomb and exchange potentials in each SCF cycle, by the accurate and efficient numerical integration[30,31] of the Hamiltonian matrix elements, and by the possibility to freeze core orbitals. The LSD exchange correlation potential was used,[32] with the Vosko–Wilk–Nusair[33] parametrization of the electron gas data for the local density approximation of the correlation energy. Becke's nonlocal corrections[34,35] to the exchange energy and Perdew's nonlocal corrections[36,37] to the correlation energy were used. A double-ζ STO basis set for H, C, N, and O was used, and a triple-ζ STO basis set for Ru and Mn was employed. The calculations will be referred to, in the remainder of this paper, as "DFT-MO calculations", since the Kohn–Sham formulation of density functional theory leads to molecular orbitals with a good physical basis that can be used very well in MO theoretical considerations.[38] All bases were augmented with one polarization function. Oscillator strengths (f_{calc}) were calculated using the program Dipole[39] with separately optimized excited state orbitals. The calculations were restricted to those transitions which are expected to contribute considerably to the absorption spectrum of the complex.

The structural parameters used for the DFT-MO calculations of $Ru(Me)(Mn(CO)_5)(CO)_2$(H-DAB) and $Ru(Mn(CO)_5)_2(CO)_2$(H-DAB) are based on the crystal structures of $Ru(Me)(Mn(CO)_5)(CO)_2$(iPr-PyCa),[13] $Ru(SnPh_3)_2(CO)_2$(iPr-DAB),[14] and $Ru(Re(CO)_5)_2(CO)_2$(iPr-DAB).[22]

The experimentally determined oscillator strengths (f_{exp}) for the visible absorption band were calculated using the equation $f_{exp} = 4.319 \times 10^{-9} \epsilon_{max} \Delta\tilde{\nu}$.

3. Results and Discussion

3.1. Electronic Absorption and Resonance Raman Spectra. The UV–vis absorption spectra of $Ru(SnPh_3)(M(CO)_5)(CO)_2$(iPr-DAB) and $Ru(M(CO)_5)_2(CO)_2$(iPr-DAB) (M = Mn, Re) in THF at room temperature are depicted in Figures 2 and 3, respectively, and corresponding spectral data, together with those of $Ru(Me)(M(CO)_5)(CO)_2$(iPr-DAB) (M = Mn, Re), are collected in Table 1.

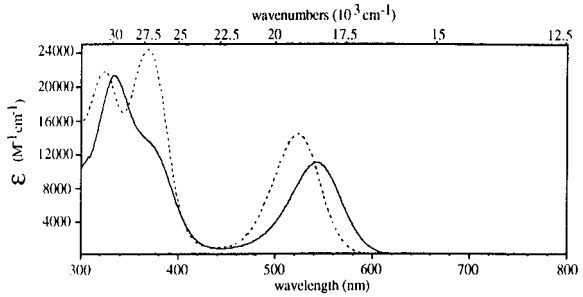

Figure 2. UV–vis spectra of $Ru(SnPh_3)(M(CO)_5)(CO)_2$(iPr-DAB) (M = Mn (—), Re (···)) measured in THF at room temperature.

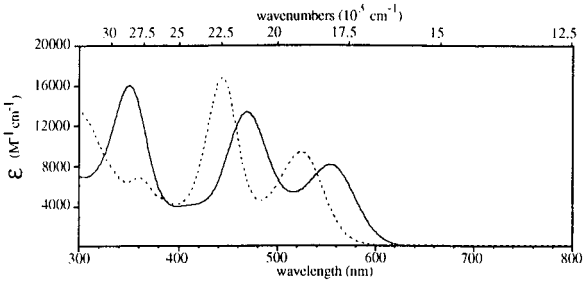

Figure 3. UV–vis spectra of $Ru(M(CO)_5)_2(CO)_2$(iPr-DAB) (M = Mn (—), Re(···)) measured in THF at room temperature.

Table 1. Parameters of the Visible Absorption Spectra of $Ru(E)(E')(CO)_2$(iPr-DAB) Measured in THF at Room Temperature: Band Maxima (λ_{max}) with Their Extinction Coefficients (ϵ) in Parentheses and Solvatochromism ($\Delta = \tilde{\nu}_{max}(CH_3(CN) - \tilde{\nu}_{max}$(hexane))

compound			
E	E′	λ_{max} (ϵ) (nm) (M^{-1} cm^{-1})	Δ (cm^{-1})
$SnPh_3$	$Mn(CO)_5$	542 (10 980)	440
Me	$Mn(CO)_5$	558 (13 000)[a]	944[a]
$Mn(CO)_5$	$Mn(CO)_5$	467 (13 247)/554(8064)	−185/387
$SnPh_3$	$Re(CO)_5$	524 (8269)	327
Me	$Re(CO)_5$	541 (14 075)	508
$Re(CO)_5$	$Re(CO)_5$	444 (16 653)/524 (9278)	−103/146

[a] From ref 13.

The complexes $Ru(SnPh_3)(M(CO)_5)(CO)_2$(iPr-DAB) and $Ru(Me)(M(CO)_5)(CO)_2$(iPr-DAB) (M = Mn, Re) exhibit a single intense visible band whose position is only weakly affected by the axial ligands (E or E′), Table 1. Both the extinction coefficient (ϵ) and solvatochromism of this band are higher for E = Me than for E = $SnPh_3$.

On the other hand, the spectra of both trinuclear complexes $Ru(M(CO)_5)_2(CO)_2$(iPr-DAB) show two visible absorption bands. The wavelength of the maximum of the lowest-energy band increases on going from $Ru(Re(CO)_5)_2(CO)_2$(iPr-DAB) to $Ru(Mn(CO)_5)_2(CO)_2$(iPr-DAB).

To assign the visible absorption band(s), the UV–vis data were supplemented with the resonance Raman (rR) spectra and DFT-MO calculations. The use of rR spectra to characterize allowed electronic transitions is based on the fact[40] that only those Raman peaks are enhanced in intensity which correspond to vibrations whose normal coordinates are affected by the resonant electronic transition. Strong emission, especially for the $Re(CO)_5$-containing complexes, restricted the measure-

(25) Worl, L. A.; Duesing, R.; Chen, P.; Della Ciana, L.; Meyer, T. J. *J. Chem. Soc., Dalton Trans.* **1991**, 849.
(26) Parker, C. A.; Rees, W. T. *Analyst (London)* **1960**, *85*, 587.
(27) Caspar, J. V.; Meyer, T. J. *J. Am. Chem. Soc.* **1983**, *105*, 5583.
(28) Baerends, E. J.; Ellis, D. E.; Ros, P. *Chem. Phys.* **1973**, *2*, 52.
(29) Baerends, E. J.; Ros, P. *Int. J. Quantum Chem.* **1978**, *S12*, 169.
(30) Boerrigter, P. M.; te Velde, G.; Baerends, E. J. *Int. J. Quantum Chem.* **1988**, *33*, 87.
(31) te Velde, G.; Baerends, E. J. *J. Comput Phys.* **1992**, *99*, 84.
(32) Parr, R. G.; Yang, W. *Density Functional Theory of Atoms and Molecules*; Oxford University Press: New York, 1989.
(33) Vosko, S. H.; Wilk, L.; Nusair, M. J. *Can. J. Phys.* **1980**, *58*, 1200.
(34) Becke, A. D. *J. Chem. Phys.* **1986**, *84*, 4524.
(35) Becke, A. D. *Phys. Rev.* **1988**, *A38*, 3098.
(36) Perdew, J. P. *Phys. Rev.* **1986**, *B33*, 8822.
(37) Perdew, J. P. *Phys. Rev.* **1986**, *B34*, 7406.
(38) Baerends, E. J.; Gritsenko, O. V.; van Leeuwen, R. In *Chemical Applications of Density-Functional Theory*; Laird, B. B., Ross, R., Ziegler, T., Eds.; ACS Symposium Series 629; American Chemical Society: Washington, DC, 1996; p 20.
(39) Wilms, M. P. Internal report, Free University Amsterdam, 1995.
(40) Clark, G. R.; Flower, K. R.; Roper, W. R.; Wright, L. J. *Organometallics* **1993**, *12*, 259.

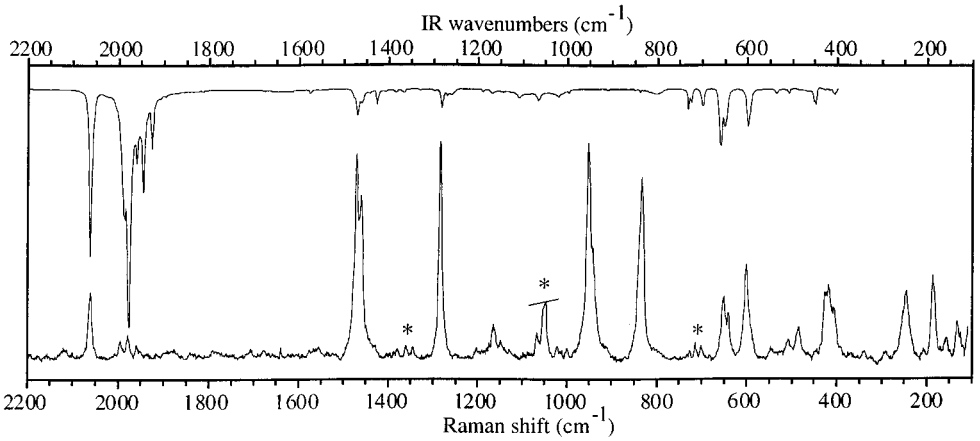

Figure 4. IR (KBr) and rR (*KNO_3, λ_{exc} = 476.5 nm) spectra of $Ru(SnPh_3)(Mn(CO)_5)(CO)_2$(iPr-DAB).

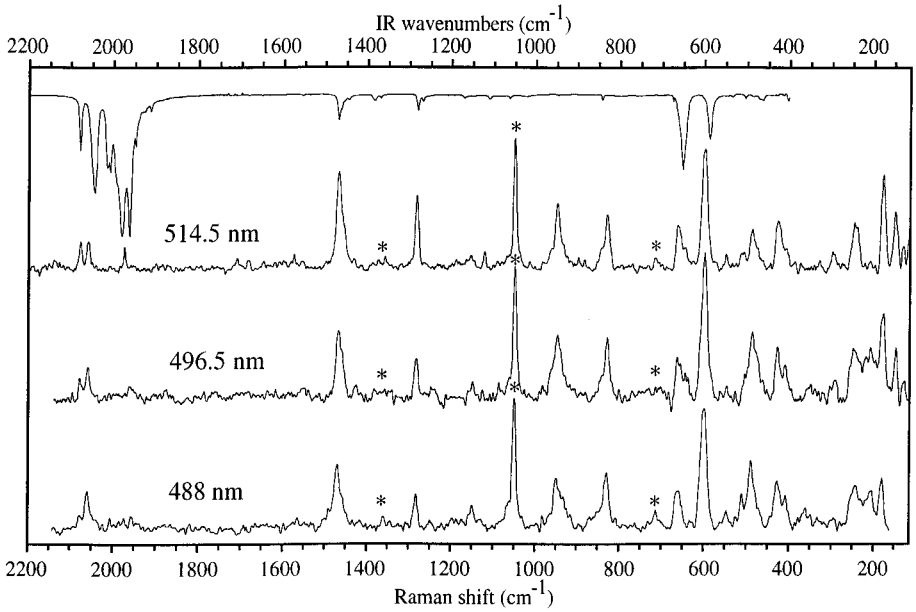

Figure 5. IR (KBr) and rR (*KNO_3, λ_{exc} = 514.5, 496.5, 488 nm) spectra of $Ru(Mn(CO)_5)_2(CO)_2$(iPr-DAB).

ments to excitation wavelengths at the high-energy side of the absorption band and to a relatively narrow wavenumber region, 100-1800 cm^{-1}. All Raman bands observed show a monotonic increase of intensity when the excitation wavelength approaches the maximum of the absorption band, indicating their resonant enhancement. A complete list of the rR peak wavenumbers has been published elsewhere.[22]

Shown in Figures 4−6 are rR spectra of $Ru(SnPh_3)(Mn(CO)_5)(CO)_2$(iPr-DAB), $Ru(Mn(CO)_5)_2(CO)_2$(iPr-DAB), and $Ru(Re(CO)_5)_2(CO)_2$(iPr-DAB), respectively. The rR spectroscopic patterns of all complexes studied are very similar and resemble those of $Re(M(CO)_5)(CO)_3$(iPr-DAB) (M = Mn, Re).[41] Strong resonance enhancement of the ν_s(CN) band at *ca.* 1470 cm^{-1} indicates that the resonant electronic transition is directed to the π^* orbital of the DAB ligand. The concomitant rR effects of the ν(C−C) vibration (*ca.* 1270 cm^{-1}), of the DAB deformation vibrations at *ca.* 950 and 830 cm^{-1}, and of skeletal vibrations (δ(M−C−O), ν(M−C), ν(M−N), and, possibly, ν(M−M′)) in the region below 700 cm^{-1} are very characteristic of a highly delocalized resonant electronic transition that involves orbitals of a mixed Ru(E)(E′) and DAB character.[15,22,41] The structural effects of this transition are distributed over many normal coordinates, giving rise to rR effects for both ligand and skeletal vibrations. The spectra shown also show a rR effect for ν(CO) bands at 2050−2100 cm^{-1}. The wavenumbers of these resonance-enhanced vibrations are higher than those measured for the ν(CO) vibrations in the related complexes Ru(E)(E′)$(CO)_2$(iPr-DAB), where E, E′ ≠ $M(CO)_5$.[42,43] Hence, these Raman peaks are assigned to ν(CO) vibrations of the $M(CO)_5$ groups.

The rR spectra of $Ru(SnPh_3)(Mn(CO)_5)(CO)_2$(iPr-DAB) show a single strong ν(CO) band at 2065 cm^{-1} (Figure 4), whereas the spectra of $Ru(M(CO)_5)_2(CO)_2$(iPr-DAB) (M = Mn, Re) show two closely spaced ν(CO) vibrations in this region (2082, 2051 cm^{-1} for M = Mn and 2105, 2079 cm^{-1} for M = Re) (see Figures 5 and 6). The bands are tentatively assigned to two conformers. This assignment is supported by the observation of these bands with comparable intensities in the IR spectra, by the

(41) Kokkes, M. W.; Snoeck, T. L.; Stufkens, D. J.; Oskam, A.; Christophersen, M.; Stam, C. H. *J. Mol. Struct.* **1985**, *131*, 11.

(42) Aarnts, M. P.; Stufkens, D. J.; Oskam, A.; Fraanje, J.; Goubitz, K. *Inorg. Chim. Acta* In press.

(43) As was already shown for Ru(Cl)(Me)$(CO)_2$(iPr-DAB) and Ru(Cl)$(SnPh_3)(CO)_2$(iPr-DAB), the atomic orbital contributions to the MOs of both complexes are very similar, except for the increased admixture of the Cl−Ru−Sn σ-bonding orbital into the DAB π^* orbital compared with that of the Cl−Ru−Me σ-bonding orbital.[47]

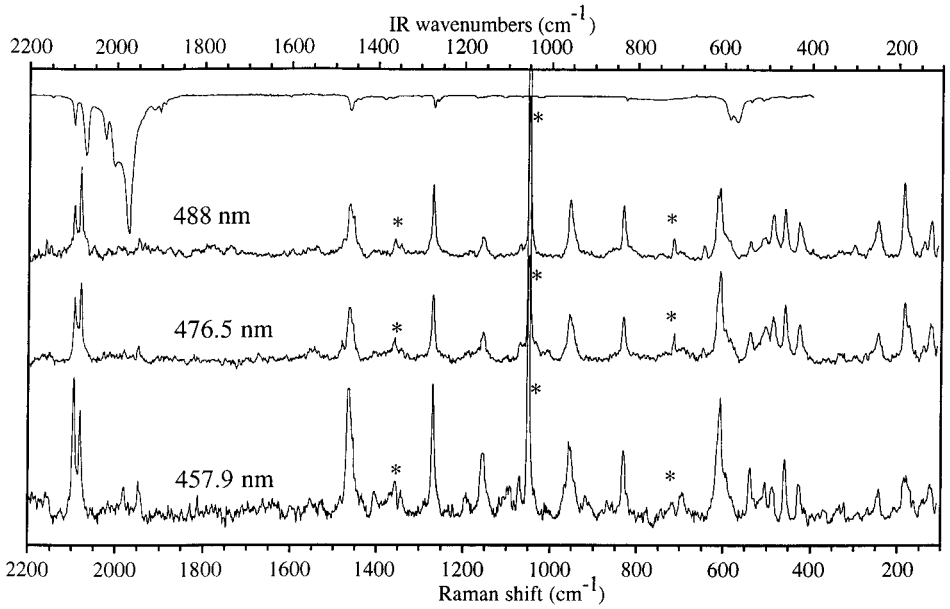

Figure 6. IR (KBr) and rR (*KNO_3 λ_{exc} = 488, 476.5, 457.9 nm) spectra of $Ru(Re(CO)_5)_2(CO)_2$(iPr-DAB).

Table 2. Characters and Energies of the Relevant MOs[a] of Ru(Me)(Mn(CO)$_5$)(CO)$_2$(H-DAB) (A) and Ru(Mn(CO)$_5$)$_2$(CO)$_2$(H-DAB) (B), As Calculated by DFT

compound	orbital	description	ϵ (eV)	Ru	Mn(CO)$_5$[b]	H-DAB	CO (of Ru)
A	**42a′**	**π*DAB**	**−4.063**	**7% d_{yz}**	**29% 10a$_1$ (d_{z^2})**	**58% 2b$_1$**	**7% 2π**
	41a′	**σ Ru−Mn**	**−5.609**	**8% p_z**	**48% 10a$_1$ (d_{z^2})**	**24% 2b$_1$**	
	24a″	dt_{2g}Ru	−5.975	67% d_{xz}	7% 8e (d_{xz})	10% 1a$_2$	
	40a′	dt_{2g}Ru[c]	−6.426	51% d_{yz}	26% 8e (d_{yz})	8% 2b$_1$	7% 2π
B	**27b$_1$**	**π*DAB**	**−4.061**	**7% d_{yz}**	**34% 10a$_1$(d_{z^2})−**	**58% 2b$_1$**	
	26b$_1$	**σ_n Ru−Mn**	**−5.642**	**6% p_z**	**58% 10a$_1$(d_{z^2})−**	**25% 2b$_1$**	
	14a$_2$	dt_{2g}Ru	−6.029	65% d_{xz}		10% 1a$_2$	11% 2π
	25b$_1$	dt_{2g}Ru[c]	−6.431	49% d_{yz}	32% (d_{yz})−	5% 2b$_1$	9% 2π
	34a$_1$	σ_b Ru−Mn	−6.699	6% 5s, 44% d_{z^2}	45% 10a$_1$(d_{z^2})+		

[a] Only those orbitals are presented which are involved in the low-energy transitions. The HOMO (41a′ and 26b$_1$) and LUMO (42a′ and 27b$_1$) orbitals are printed boldface type. [b] The orbital in parentheses specifies the principal contributing Mn d orbital. Symbols + and − denote their symmetric and antisymmetric combinations, respectively. [c] An alternative description of these orbitals is π* Ru−Mn, since there is a considerable mixing between the Ru and Mn orbitals.

Table 3. Electronic Transitions to the Lowest ^{1}A′ Excited States of Ru(Me)(Mn(CO)$_5$)(CO)$_2$(H-DAB) (A) and of Ru(Mn(CO)$_5$)$_2$(CO)$_2$(H-DAB) (B): Changes in Mulliken Populations, Transition Energies, and Oscillator Strengths, As Calculated by DFT

compound/ transition	Ru p_z	Ru d_{z^2}	Ru d_{xy}	Ru d_{yz}	DAB a$_1$	DAB b$_1$	DAB b$_2$	CO π[a]	Mn a$_1$[b]	Mn e[b]	Me	E^{1}A′ (cm^{-1} (nm))	E^{3}A′ (cm^{-1} (nm))	f_{cal}[c]	f_{exp}[d]
A GS	2.17	0.99	0.64	1.54	10.03	2.75	7.67	9.05	19.08	32.03	7.23				
41a′ → 42a′	−0.10	**+0.05**	+0.02	**−0.02**	−0.05	**+0.24**	−0.03	−0.04	**−0.07**	+0.02	−0.05	14 218 (703)	11 283 (886)	0.1640	0.1236[e]
40a′ → 42a′	−0.01	**+0.07**	+0.06	**+0.26**	−0.07	**+0.35**	−0.07	−0.09	**+0.36**	+0.02	+0.06	20 153 (496)	19 634 (509)	0.0702	
B GS	2.19	1.10	0.66	1.52	9.99	2.76	7.66	9.08	38.02	64.03					
26b → 27b$_1$	**−0.07**	−0.03	+0.01	**+0.08**	−0.03	**+0.23**	−0.04	−0.02	**−0.12**	+0.05		14 424 (693)	11 785 (850)	0.082	0.093[f]
25b$_1$ → 27b$_1$	0.00	+0.09	+0.03	**−0.29**	−0.03	**+0.33**	−0.08	−0.09	**+0.36**	**−0.32**		20 630 (485)	19 759 (506)	0.058	
34a$_1$ → 27b$_1$	+0.01	**−0.30**	+0.04	**+0.16**	−0.06	**+0.37**	−0.08	−0.04	**−0.10**	+0.05		21 979 (455)	21 549 (464)	0.200	0.159[g]

[a] COs of ruthenium. [b] Mn = Mn(CO)$_5$. [c] Oscillator strength calculated with separately optimized excited state orbitals. [d] Calculated for Ru(Me)(Mn(CO)$_5$)(CO)$_2$(iPr-DAB) and Ru(Mn(CO)$_5$)$_2$(CO)$_2$(iPr-DAB) using the equation $f = 4.319 \times 10^{-9}\ \epsilon_{max}\Delta\nu$ ($\Delta\nu$ = width at half-height). [e] Band at 558 nm (= 17 921 cm^{-1}). [f] Band at 554 nm (= 18 050 cm^{-1}). [g] Band at 467 nm (= 21 413 cm^{-1}).

rapid change of their relative intensities over a small wavelength region due to nearly coinciding electronic transitions, and by the observation of a similar, although much smaller, splitting for the ν_s(CN) Raman band.

3.2. DFT-MO Calculations. In Tables 2 and 3 and Figures 7 and 8, the calculated orbital contributions, chosen axes orientations, energy differences, and MO diagrams, obtained from the DFT-MO calculations, are presented for the model compounds Ru(Me)(Mn(CO)$_5$)(CO)$_2$(H-DAB) and Ru(Mn(CO)$_5$)$_2$(CO)$_2$(H-DAB), respectively. These data are used to describe the bonding in Ru(SnPh$_3$)(Mn(CO)$_5$)(CO)$_2$(iPr-DAB)[43] and Ru(Mn(CO)$_5$)$_2$(CO)$_2$(iPr-DAB), with a possible qualitative generalization to Ru(E)(E′)(CO)$_2$(iPr-DAB) (E = SnPh$_3$, Me; E′ = Mn(CO)$_5$, Re(CO)$_5$) and Ru(Re(CO)$_5$)$_2$(CO)$_2$(iPr-DAB), respectively. To simplify the description, the orbitals of the Mn(CO)$_5$ fragment (8e, 2b$_1$, 6b$_1$, 10a$_1$) will be described by their principal Mn d component.

According to these calculations, the LUMO of Ru(Me)(Mn(CO)$_5$)(CO)$_2$(H-DAB) as well as Ru(Mn(CO)$_5$)$_2$(CO)$_2$(H-DAB) is mainly composed of the π* orbital of the DAB ligand, with an admixture of the $\sigma_{(Ru-Mn)}$ orbital for Ru(Me)(Mn(CO)$_5$)(CO)$_2$(H-DAB) and a delocalized $\sigma_{(Mn-Ru-Mn)}$ orbital for Ru(Mn(CO)$_5$)$_2$(CO)$_2$(H-DAB). The HOMO of Ru(Me)(Mn(CO)$_5$)(CO)$_2$(H-DAB) consists

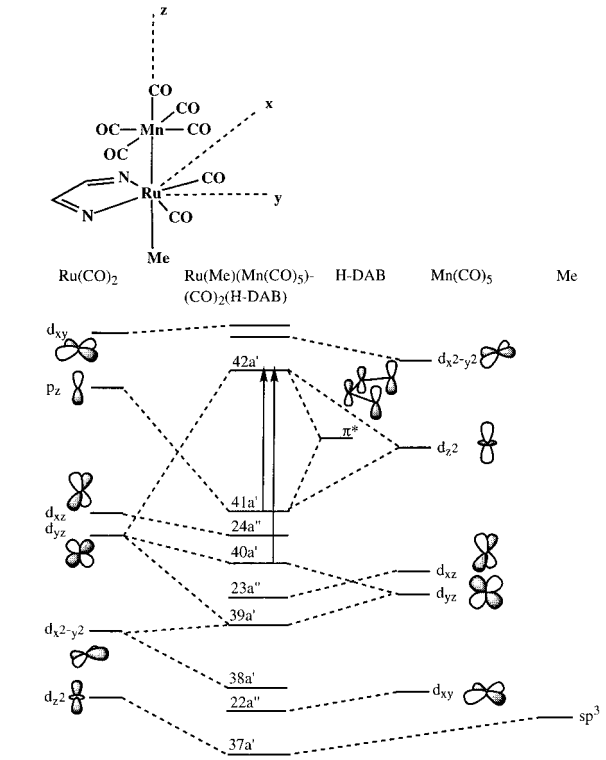

Figure 7. Qualitative MO scheme of Ru(Me)(Mn(CO)$_5$)-(CO)$_2$(H-DAB) based on the DFT-MO calculations. The vertical arrows show the principal electronic transitions discussed in the text and presented in Table 3.

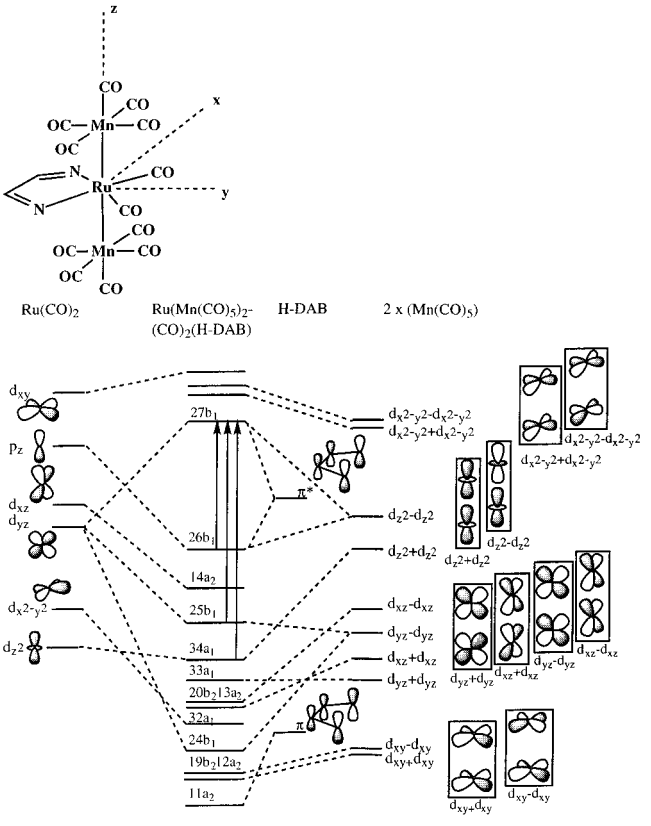

Figure 8. Qualitative MO scheme of Ru(Mn(CO)$_5$)$_2$(CO)$_2$-(H-DAB) based on the DFT-MO calculations. The vertical arrows show the principal electronic transitions discussed in the text and presented in Table 3.

mainly of the Ru(p_z) + Mn(d_{z^2}) orbital, which is σ-bonding with respect to the axial Ru−Mn bond. For Ru(Mn(CO)$_5$)$_2$(CO)$_2$(H-DAB), the HOMO (26b$_1$) has the composition (Ru(p_z) + (Mn(d_{z^2}) − Mn(d_{z^2})) + H-DAB(π*)). It originates in the interaction of the Ru(5p_z) orbital with the antisymmetric combination of the d_{z^2} orbitals of the axially bound Mn atoms. It has a nearly σ-nonbonding (or very weakly bonding) character with respect to the Mn−Ru−Mn bonds. The strongly Mn−Ru−Mn σ-bonding orbital 34a$_1$, which has the composition (Ru(d_{z^2}) + Mn(d_{z^2}) + Mn(d_{z^2})), lies somewhat lower in energy. Hereinafter, the 26b$_1$ σ-nonbonding and the 34a$_1$ σ-bonding orbitals of Ru(Mn(CO)$_5$)$_2$(CO)$_2$(H-DAB) will be denoted σ_n and σ_b, respectively. Evidently, the axial Mn−Ru−Mn bond in Ru(Mn(CO)$_5$)$_2$(CO)$_2$(H-DAB) is a delocalized three-center σ bond, similar to the Sn−Ru−Sn bond in Ru(SnH$_3$)$_2$(CO)$_2$(H-DAB).[14] Importantly, the calculations indicate for both complexes a rather large mixing between the atomic orbitals involved in the axial σ-bonding and the π* 2b$_1$ orbital of DAB in the HOMO (see Table 2). This implies a donation of σ electron density from the Ru(E)(E′) unit to the π* orbital of the DAB ligand. This $\sigma\pi$* delocalization is a rather unusual type of π back-bonding. It appears to be quite characteristic of Ru(E)(E′)(CO)$_2$(iPr-DAB) complexes, in which both E and E′ are covalently bound via energetically high-lying σ orbitals.[14]

The axial σ Me−Ru−Mn bond of Ru(Me)(Mn(CO)$_5$)-(CO)$_2$(H-DAB) is not delocalized like that in Ru(Mn-(CO)$_5$)$_2$(CO)$_2$(H-DAB) or Ru(E)(E′)(CO)$_2$(H-DAB) (E = SnPh$_3$, E′ = Me, SnPh$_3$).[14,42] Instead, it should be viewed as composed of two localized σ bonds, Ru−Mn and Ru−Me, respectively. A smaller contribution to the HOMO is also expected for the Sn fragment compared with the contributions from Mn or Re in the Ru(SnPh$_3$)-(M(CO)$_5$)(CO)$_2$(iPr-DAB) (M = Mn, Re) complexes.

The HOMO-1 of Ru(Mn(CO)$_5$)$_2$(CO)$_2$(H-DAB) is essentially a Ru(dπ) orbital, and the HOMO-2, which might be of spectroscopic importance, has a Mn−Ru−Mn π-antibonding character. A similar repulsive Ru−Mn π interaction takes place for Ru(Me)(Mn(CO)$_5$)(CO)$_2$-(H-DAB) in the 40a′ and 39a′ orbitals (see Table 2). The HOMO-3 of Ru(Mn(CO)$_5$)$_2$(CO)$_2$(H-DAB) is the 34a$_1$ orbital (σ_b), which lies energetically still high enough to be possibly involved in low-energy transitions, *vide infra*.

3.3. Assignment of the Visible Absorption Bands. Calculated transition energies and oscillator strengths (f) of the relevant electronic transitions are presented in Table 3. The a″ → a′ or a$_2$ → b$_1$ transitions were calculated to be too weak (f < 0.001) to contribute to the experimental spectra.

Based on the DFT-MO calculations, the lowest absorption band of Ru(E)(M(CO)$_5$)(CO)$_2$(iPr-DAB) (E = Me, SnPh$_3$; M = Mn, Re) as well a that of Ru(M(CO)$_5$)$_2$-(CO)$_2$(iPr-DAB) (M = Mn, Re) may be assigned straightforwardly to the HOMO → LUMO transition of $\sigma \rightarrow \pi$* or $\sigma_n \rightarrow \pi$* character, respectively.[44] The surprisingly high values of the oscillator strengths appear to result from the large delocalization of the HOMO and LUMO, which both consist of contributions from essentially the

(44) The calculations predict the $\sigma \rightarrow \pi$* and $\sigma_n \rightarrow \pi$* transitions of the model compounds Ru(Me)(Mn(CO)$_5$)(CO)$_2$(H-DAB) and Ru(Mn-(CO)$_5$)$_2$(CO)$_2$(H-DAB), respectively, to occur at comparable energies, the former one being 1.9 times more intense. In agreement with this, the spectra of the corresponding iPr-DAB complexes showed absorption bands at *ca.* 18 000 cm^{-1} with a ratio of 1.6 for their extinction coefficients.

Table 4. Emission Properties of Ru(E)(E′)(CO)$_2$(iPr-DAB) in a 2-Me-THF Glass at 80 K

compound			λ_{exc} = 460 nm						λ_{exc} = 532 nm		
E	E′	λ_{abs} (nm)	λ_{em} (nm)	ΔE^a (cm^{-1})	τ (μs)	Φ_r ($\times 10^{-4}$)	k_r (s^{-1})	k_{nr} ($\times 10^4$ s^{-1})	λ_{em} (nm)	ΔE^a (cm^{-1})	τ (μs)
$SnPh_3$	$Mn(CO)_5$	518	683	4663	4.1	1.2	29	24	850	7540	~10
Me[b]	$Mn(CO)_5$	529	832	6884	~10	~0.07	~0.7	~10			
$SnPh_3$	$Re(CO)_5$	509	742	6169	90	22.5	25	1.1	755	6401	37
Me	$Re(CO)_5$	518	780	6485	~26	~0.7	~2.7	~3.8	~810	6959	~9
$Re(CO)_5$	$Re(CO)_5$	512	770	6544	46	3.2	6.9	2.2	770	6544	46

[a] Apparent Stokes shift ($\Delta E = \tilde{\nu}_{em} - \tilde{\nu}_{abs}$). [b] From ref 1.

same atomic and fragment orbitals. This highly delocalized character of the HOMO → LUMO transition, predicted by the calculations, is evident from the small solvatochromism of the first absorption band and from the resonance enhancement of Raman intensity for DAB deformation modes and Ru(DAB) skeletal vibrations (*vide supra*). The $\sigma \rightarrow \pi^*$ character of the lowest-energy transition of all complexes under study is also supported by the rR effect observed for bands between 2050 and 2100 cm^{-1}, which belong to ν(CO) vibrations of the $M(CO)_5$ groups.[22] Their enhancement implies that the $M(CO)_5$ groups are involved in the electronic transition, which agrees with its $\sigma_{n(M-Ru-M)} \rightarrow \pi^*$ or $\sigma_{(Ru-M)} \rightarrow \pi^*$ character, respectively.

The second strong absorption band found for Ru(Mn(CO)$_5$)$_2$(CO)$_2$(iPr-DAB) and Ru(Re(CO)$_5$)$_2$(CO)$_2$(iPr-DAB) at 467 and 444 nm, respectively, appears to belong to the $34a_1 \rightarrow 27b_1$ transition, since its calculated oscillator strength is quite large and it is predicted to occur at a reasonable energy for Ru(Mn(CO)$_5$)$_2$(CO)$_2$(H-DAB). Given the Mn−Ru−Mn σ-bonding character of the $34a_1$ orbital (*vide supra*, Table 2), this transition may be described as $\sigma_b \rightarrow \pi^*$. The calculation predicts this transition to be 2.4 times more intense than the lower $\sigma_n \rightarrow \pi^*$ one, which is in reasonable agreement with the ratio 1.7 of the experimentally determined oscillator strengths. Moreover, also the absolute values of these experimental oscillator strengths (f_{exp}) agree rather well with those obtained with the DFT-MO calculations (Table 3). The assignment of the high- and low-energy absorption bands of Ru(Mn(CO)$_5$)$_2$(CO)$_2$(iPr-DAB) to $\sigma_b \rightarrow \pi^*$ and $\sigma_n \rightarrow \pi^*$, respectively, agrees with the absence of solvatochromism and rigidochromism for both of these bands and with the observation of identical patterns for the Raman peaks belonging to DAB and skeletal vibrations upon excitation into either of the two absorption bands. This is because both transitions are directed to the same, highly delocalized, LUMO orbital. This is because both transitions are directed to the same, highly delocalized, LUMO orbital. Hence, the same bonds of the Ru−DAB moiety are affected by excitation, and the same vibrations are coupled to both electronic transitions.

The character of the electronic transitions responsible for the visible absorption bands of Ru(Me)(Mn(CO)$_5$)(CO)$_2$(iPr-DAB) and Ru(Mn(CO)$_5$)$_2$(CO)$_2$(iPr-DAB) is visualized by the calculated changes in the Mulliken population of the individual atomic or fragment orbitals, shown in Table 3. Thus, the $\sigma \rightarrow \pi^*$ (HOMO−LUMO) excitation of Ru(Me)(Mn(CO)$_5$)(CO)$_2$(H-DAB) depopulates the σ orbitals of Mn and Me by −0.07 and −0.05, respectively, while the electron density in the $\pi^*_{(DAB)}$ orbital increases by +0.27. The depopulation of the Me σ orbital by an amount comparable to that of Mn is noteworthy, especially in view of the fact that the σ orbital in which the transition originates is a localized Ru−Mn σ orbital, with no appreciable Me contribution (Table 3). The Me−Ru bond is apparently affected through an orbital relaxation on excitation. For Ru(Mn(CO)$_5$)$_2$(CO)$_2$(H-DAB), the lower $\sigma_n \rightarrow \pi^*$ transition depopulates the Mn σ orbitals by −0.12, while the population of the $\pi^*_{(DAB)}$ orbital increases by +0.23. Similar effects are caused by the higher $\sigma_b \rightarrow \pi^*$ transition, which, however, leads to even larger charge separation. This is because the σ_b orbital does not, for symmetry reasons, mix with the $\pi^*_{(DAB)}$ orbital. Hence, the compensating $\sigma-\pi^*$ interaction, effective in the case of the $\sigma_n \rightarrow \pi^*$ transition, is absent for $\sigma_b \rightarrow \pi^*$.

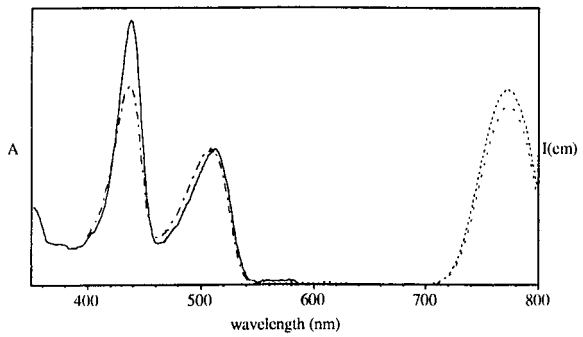

Figure 9. Absorption (—), emission, λ_{exc} = 438 nm (···), emission, λ_{exc} = 514 nm (- - -), and excitation λ_{em} = 765 nm (—·—) spectra of Ru(Re(CO)$_5$)$_2$(CO)$_2$(iPr-DAB) in a 2-MeTHF glass at 80 K.

The DFT calculations also indicate that the weaker π^*(Ru−Mn) → π^*(DAB) transitions $25b_1 \rightarrow 27b_1$ or 40a′ → 42a′ (Table 3) might be hidden under the $\sigma_b \rightarrow \pi^*$ absorption band of Ru(Mn(CO)$_5$)$_2$(CO)$_2$(iPr-DAB) or under the onset of the intense near-UV absorption of Ru(Me)(Mn(CO)$_5$)(CO)$_2$(iPr-DAB), respectively.

3.4. Time-Resolved Emission Spectra. Emission properties were studied for Ru(E)(Mn(CO)$_5$)(CO)$_2$(iPr-DAB), (E = Me, $SnPh_3$) and Ru(E)(Re(CO)$_5$)(CO)$_2$(iPr-DAB) (E = Me, $SnPh_3$, $Re(CO)_5$). Spectra of Ru(Mn(CO)$_5$)$_2$(CO)$_2$(iPr-DAB) were not measured because of its low emission quantum yield and high photolability.

All complexes studied show an unstructured emission band in a 2-MeTHF glass at 80 K. Its position slightly depends on the excitation wavelength, with the exception of that of Ru(Re(CO)$_5$)$_2$(CO)$_2$(iPr-DAB) (see Tables 1 and 4 and Figures 9 and 10).

Obviously, excitation at 460 nm at the high-energy side of the absorption band gives rise to a relatively intense emission that occurs at a slightly higher energy (by *ca.* 200−500 cm^{-1}) than the emission observed upon 532 nm excitation. The two emissions have their counterparts in the excitation spectra which show two bands at a slightly different position, hidden within the single absorption band envelope (Figure 10). Just as in the case of the rR spectra, we tentatively explain this

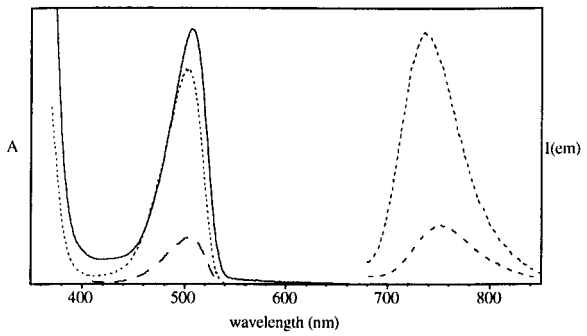

Figure 10. Absorption (—), emission, $\lambda_{exc} = 460$ nm (- - -), emission, $\lambda_{exc} = 532$ nm (- -), excitation, $\lambda_{em} = 725$ nm (•••), and excitation, $\lambda_{em} = 800$ nm (— —) spectra of $Ru(SnPh_3)(Re(CO)_5)(CO)_2$(iPr-DAB) in a 2-MeTHF glass at 80 K.

effect by the presence of two conformers, which are neither equilibrated in their ground state nor in their excited state in the rigid glass at 80 K.

The emission data (Table 4) show that all complexes studied exhibit relatively long lifetimes and small apparent Stokes shifts. Such properties are quite characteristic of the emission from a $^3\sigma\pi^*$ state[1,8,9,45] or, more precisely, from the $^3\sigma_n\pi^*$ in the case of $Ru(Re(CO)_5)_2(CO)_2$(iPr-DAB). As is common for the $^3\sigma\pi^*$ states,[6,15] the Sn-containing $Ru(SnPh_3)(Re(CO)_5)(CO)_2$(iPr-DAB) species shows a longer excited state lifetime than Ru(Me)$(Re(CO)_5)(CO)_2$(iPr-DAB). In this family of compounds, the lifetime increases (*i.e.*, the k_{nr} decreases) with increasing emission energy and decreasing Stokes shift, although the variation in the latter parameter is rather small. This suggests an identical $\sigma\pi^*$ excited state character for all the Ru(E)$(Re(CO)_5)(CO)_2$(iPr-DAB) species studied herein.

The $Ru(Re(CO)_5)_2(CO)_2$(iPr-DAB) complex, which has two low-lying absorption bands, shows only a single emission band at a relatively low energy. The excitation spectrum measured at 770 nm shows two bands whose positions match those of the two absorption bands. However, the intensity ratio between the high- and low-energy excitation bands is 1.3 times smaller than that between the corresponding absorption bands. Hence, the emitting $^3\sigma\pi^*$ state is populated less efficiently from the higher $\sigma_b\pi^*$ excited state than from the lower $\sigma_n\pi^*$ state. This relatively inefficient $\sigma_b\pi^* \rightarrow \sigma_n\pi^*$ nonradiative transition is most probably due to the different symmetries of these states.

The emission properties in fluid solution at room temperature were not investigated because of an efficient photoreactivity of these complexes, which will be described elsewhere.[46]

Conclusion

The presence of an energetically high-lying σ orbital in the axial E,E′ ligands in Ru(E)(E′)$(CO)_2$(iPr-DAB) (E = Me, $SnPh_3$, or $Mn(CO)_5$, E′ = $Mn(CO)_5$; E = Me, $SnPh_3$, or $Re(CO)_5$, E′ = $Re(CO)_5$) results in a delocalized three-center E−Ru−E′ σ bond. The HOMO of such complexes has essentially E−Ru−E′ σ-nonbonding character, σ_n. If E and E′ are not equivalent, then the σ bonding is more delocalized. This is, *e.g.*, the case for Ru(Me)$(M(CO)_5)(CO)_2$(iPr-DAB) (M = Mn, Re), where the HOMO is a Ru−M σ-bonding orbital. Another important feature of all these Ru(E)(E′)$(CO)_2$(iPr-DAB) complexes is an extensive delocalization of the E−Ru−E′ σ electron density into the π^* orbital of the DAB ligand. All the Ru(E)(E′)$(CO)_2$(iPr-DAB) complexes studied herein have a lowest $^3\sigma\pi^*$ excited state which is characterized by a rather long lifetime, slow nonradiative decay to the ground state, and small excited state distortion.

Acknowledgment. The Netherlands Foundation for Chemical Research (SON) and the Netherlands Organisation for Scientific Research (NWO), together with the COST Action D4 program and European Scientific Network "Organometallic Photochemistry", are thanked for financial support.

OM9608667

(45) Morse, D. L.; Wrighton, M. S. *J. Am. Chem. Soc.* **1976**, *98*, 3931.

(46) Aarnts, M. P.; Stufkens, D. J.; Vlček, A., Jr. *Inorg. Chim. Acta*, in press.

(47) Wilms, M. P.; Baerends, E. J.; Stufkens, D. J. To be submitted for publication.